Mean radiative energy balance and vertical mass fluxes in the equatorial upper troposphere and lower stratosphere

T. Corti, B. P. Luo, and T. Peter
Institute for Atmospheric and Climate Science, Swiss Federal Institute of Technology (ETH), Zurich, Switzerland

H. Vömel
Cooperative Institute for Research in Environmental Sciences, University of Colorado, Boulder, Colorado, USA

Q. Fu
Department of Atmospheric Sciences, University of Washington, Seattle, Washington, USA

Received 1 November 2004; revised 16 December 2004; accepted 25 January 2005; published 17 March 2005.

[1] We use radiative transfer calculations to quantify vertical mass transport in the equatorial upper troposphere (UT) and lower stratosphere (LS), employing high resolution sonde measurements of temperature, ozone and water vapor at seven equatorial locations (10°S–10°N). The influence of clouds is examined using data from the International Satellite Cloud Climatology Project (ISCCP) and the Lidar-In-Space Technology Experiment (LITE). The resulting mean heating rate profiles show that the transition from radiative cooling to heating occurs significantly lower in the full sky case than in the clear sky case, demonstrating the importance of clouds for processes in the UT, such as troposphere-to-stratosphere transport (TST). The heating rate profiles are used to calculate mean vertical mass fluxes, which show a divergent mass flux from 15–19 km. This suggests that only a small part of the air ascending through the cold point tropopause can reach the middle stratosphere. Above 19 km the vertical motion is a non-divergent upwelling mass flux consistent with the idea of a Brewer-Dobson circulation driven by waves dissipating in the extratropical stratosphere. Lower down, other processes are also responsible for the upwelling. **Citation:** Corti, T., B. P. Luo, T. Peter, H. Vömel, and Q. Fu (2005), Mean radiative energy balance and vertical mass fluxes in the equatorial upper troposphere and lower stratosphere, *Geophys. Res. Lett.*, *32*, L06802, doi:10.1029/2004GL021889.

1. Introduction

[2] Upwelling in the tropical UT has been identified as responsible for most of the air entering the stratospheric overworld [*Holton et al.*, 1995]. The altitude dependence of mass fluxes involved in TST determines the composition of the air reaching the stratosphere. In the upward branch of the Hadley circulation, air is lifted from the surface into the tropical UT by deep convection, driven by latent heat release. It remains yet unclear how the air from there reaches the stratosphere. While there have been reports of convection directly reaching the tropical stratosphere [e.g., *Danielsen*, 1993], such cases seem to be quite rare. Other explanations for vertical transport of air into the stratosphere involve large-scale upwelling, possibly confined to a specific "fountain" region [*Newell and Gould-Stewart*, 1981]. *Holton et al.* [1995] have proposed that this motion is driven by waves dissipating in the extratropical stratosphere, acting like a suction pump on the tropical tropopause region.

[3] The magnitude of mean vertical mass flux changes considerably with altitude, since the Hadley circulation is much stronger than the Brewer-Dobson circulation. A variety of studies have estimated the magnitude of vertical mass flux near the tropical tropopause employing different methods. The transformed Eulerian-mean (TEM) framework has been used to derive residual mass fluxes either by solving the momentum and continuity equations based on global circulation model (GCM) simulations [e.g., *Rosenlof and Holton*, 1993] or by calculating the terms of the thermodynamic equation based on radiative heating rate calculations applied to satellite data [e.g., *Eluszkiewicz et al.*, 1996]. Alternatively, studies based on the evaluation of the tape recorder signal ($2[CH_4] + [H_2O]$) and measurements of other tracers provided profiles of mean vertical mass fluxes above the cold point tropopause [e.g., *Mote*, 1998; *Boering et al.*, 1996]. All studies found a zonal mean upward mass flux of 1–2 kg m^{-2} day^{-1} in the equatorial LS, decreasing with increasing altitude above the equatorial tropopause. *Rosenlof et al.* [1997] pointed out that this divergent mass flux cannot be explained by the wave driven Brewer-Dobson circulation and that therefore the base of the overworld would be higher than previously thought. With the exception of GCM based studies all studies were confined to the stratosphere.

[4] The mean energy balance of the equatorial UTLS above 15 km is approximately a balance between radiative heating and adiabatic cooling from upwelling motion. In clear sky, heating rates can be calculated accurately based on highly resolved vertical profiles of temperature, ozone and water vapor. *Gettelman et al.* [2004] have characterized the mean clear sky radiative energy balance of the equatorial UTLS, finding radiative cooling below and heating above 15 km altitude. For a more general discussion of the atmospheric radiative energy balance, clouds have to be taken into account, as they can alter the radiative energy balance of atmospheric layers [*Sohn*, 1999].

[5] In this study, we examine the full sky radiative energy balance of the equatorial UTLS including the radiative

0094-8276/05/2004GL021889$05.00

effect of clouds with high vertical resolution and the resulting mean vertical mass fluxes.

2. Data and Method

2.1. Equatorial UTLS Energy Balance

[6] The thermodynamic equation for an atmospheric layer at a given location and altitude may be written as follows [*Trenberth*, 1993]:

$$\frac{\partial T}{\partial t} = -\mathbf{v} \cdot \nabla T - w\frac{T}{\theta}\frac{\partial \theta}{\partial z} + Q. \quad (1)$$

[7] The term on the left hand side of equation (1) represents the temperature tendency. The first two terms on the right hand side are the horizontal and vertical heat advection respectively. The last term summarizes diabatic heating from latent heat release, radiation and turbulent mixing.

[8] The thermodynamic equation can be simplified under certain circumstances. We have used European Centre for Medium range Weather Forecasts (ECMWF) ERA-15 reanalysis data to estimate mean values for all components of the thermodynamic equation averaged over annual timescales and the whole equatorial belt. Our analysis has shown that the temporal mean thermodynamic equation for the equatorial UTLS can be reduced to a balance between the vertical motion term and the radiative heating term ($\overline{Q}_{rad}$),

$$\overline{w}\frac{\overline{T}}{\overline{\theta}}\frac{\overline{\partial \theta}}{\partial z} = \overline{Q}_{rad} + \overline{\epsilon}, \quad (2)$$

where the bars indicate horizontal and temporal averaging. $\overline{w}$ is the mean vertical velocity. The last term on the right hand side of equation (2) incorporates latent heat release, turbulent vertical, and both turbulent and advective meridional heat transport. We estimate $\overline{\epsilon} < 0.05$ K/day from the ECMWF ERA-15 reanalysis data for altitudes above 15 km, so that $\overline{\epsilon} \ll \overline{Q}_{rad}$, and radiative heating or cooling dominates the diabatic heating term. Below 15 km, diabatic heating due to latent heat release and turbulent vertical mixing becomes important.

[9] It is helpful to calculate vertical motion as vertical mass fluxes $M = w\rho$ rather than vertical velocity w, because M is conserved with altitude in a non-divergent flux field.

2.2. Atmospheric Profile Data

[10] Vertical profiles of temperature, ozone and water vapor with a vertical resolution of 250 m were established from various data sources. 15 profiles of water vapor up to an altitude of 28 km were taken from balloon soundings with a frost point hygrometer at San Cristóbal in different seasons [*Vömel et al.*, 2002]. A total of 985 simultaneously measured temperature and ozone profiles were taken from soundings at all equatorial Southern Hemisphere Additional Ozonesondes (SHADOZ) network locations (Figure 1) but Nairobi (because this high altitude station seems to show a clear orographic influence of Mt. Kenya on the profiles) [*Thompson et al.*, 2003a, 2003b]. All profiles from 1998–2003 without major gaps up to 28 km were used. We performed calculations with H_2O from each of the 15 balloon soundings at San Cristóbal and found a mean H_2O profile sufficient, as H_2O plays a minor role in the radiative energy balance in the UTLS (uncertainty for mean heating rate < 0.01 K/day; for the level of zero radiative heating < 50 m). All profiles have been extended to 0.1 hPa using monthly mean profiles from satellite measurements of water vapor and ozone [*Randel et al.*, 1998]. The temperature above 28 km has been set to monthly mean values from United Kingdom Meteorological Office (UKMO) analyses.

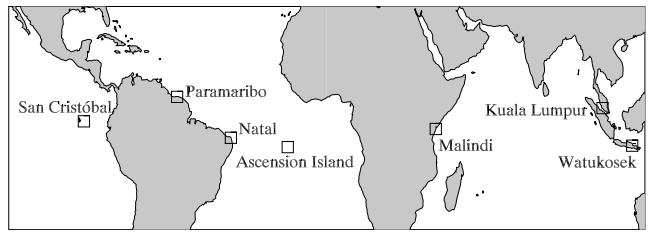

Figure 1. Locations of radiosonde measurements.

2.3. Cloud Information

[11] Two data sets on the occurrence and properties of clouds were used. The first set was derived from the ISCCP D1 data [*Rossow and Schiffer*, 1999], which is based on the analysis of weather satellite images. Every measured pixel (30 km × 30 km) is classified as either clear sky or containing a cloud, resulting in statistics on the occurrence frequency of 42 different cloud types, classified by cloud top pressure and cloud optical depth. The mean cloud distribution for the equatorial region was calculated from September 1983 to September 2001.[1]

[12] The total cloud cover in this distribution amounts to 63.2%, implying 36.8% clear sky. For calculation based on the ISCCP data set alone we assumed the cloud distribution within each individual ISSCP type to be uniform regarding cloud top pressure and optical depth. The highest cloud tops were located near the mean equatorial cold point at 95 hPa, corresponding to 17 km in the mean equatorial atmospheric profile. As ISCCP cannot distinguish between single and multiple cloud layers, all clouds were assumed to be single cloud layers with a climatological distribution of vertical extent [*Liou*, 1992; *Wang et al.*, 1998]. The missing information on detailed cloud vertical structure is a serious limitation for radiative computations. To establish an improved data set we have combined the ISCCP D1 data with cloud information from LITE, a backscatter lidar flown in space from 10–19 September 1994 [*Winker et al.*, 1996]. Despite its short measurement period, LITE provides excellent global information on vertical structure of the optically thin high clouds, which we use to refine the ISCCP cloud distribution.

[13] The lidar signals were inverted using the modified lidar equation proposed by *Volger et al.* [2002], which accounts for multiple scattering effects. Ice clouds were assumed above 7 km and water clouds below. A cloud was defined as every backscatter signal 10 times above noise. For cloud layers with optical depth $\tau < 0.1$, τ was estimated from the signal using a fixed extinction to backscatter ratio (S_c = 40), which was derived from the analysis of denser

[1] Auxiliary material is available at ftp://ftp.agu.org/apend/gl/2004GL021889.

clouds (showing no dependence on optical depth, auxiliary material). For denser clouds, the extinction to backscatter ratio was estimated from the clear sky signal below the cloud layer. We constrained the analysis to the high gain data, so that thin high clouds could be unambiguously characterized. From this we estimate that a cloud layer of 500 m thickness has a minimum detectable τ of about 4×10^{-3}.

[14] The results from this analysis are in good agreement with cloud top statistics from ground based lidar at Nauru [*Comstock et al.*, 2002] (auxiliary material). Also, 55% of the LITE profiles have $\tau < 1.27$, comparable to 53% from the ISCCP data (auxiliary material). In all cases with $\tau < 1.27$ the complete extinction profiles were used for the radiative calculation, replacing the ISCCP types with the lowest optical depths. In all cases with $\tau > 1.27$, the LITE extinction profile was used from the top-of-atmosphere down to the altitude where $\tau = 1.0$. There, a cloud was inserted downward according to the occurrence frequency for denser clouds from the ISCCP cloud distribution. The vertical extent for these clouds was again set to climatological distribution.

2.4. Radiative Transfer Calculations

[15] A radiation model by *Fu and Liou* [1992], employing the δ-four-stream approximation, was used to calculate the radiation transfer. Clear sky radiative heating rate profiles were calculated based on every profile at the seven SHADOZ locations. In each case we accounted for the solar diurnal variation of the day within which the profiles were measured. In total 985 heating rate profiles were calculated, then averaged for each location and then averaged to obtain a mean equatorial profile.

[16] The influence of clouds on the radiative heating rate profile was examined using a procedure similar to the one employed by *Hartmann et al.* [2001] (auxiliary material). A mean atmospheric profile (T, O_3, H_2O) from all balloon sonde measurements described above was used for the calculation. Heating rate profiles were calculated for each of the 42 ISCCP cloud types with further subdivisions every 250 m for cloud top altitudes and 5 steps in optical depth, adding up to 1700 radiative transfer calculations. The results for all cloud types were then weighted according to its occurrence frequency. It was finally taken into account that 36.8% of the time was clear sky. For the combined LITE-ISCCP data set, a radiative transfer calculation was performed for every of the 11,020 extinction profiles and the mean heating rate profile computed subsequently.

3. Results and Discussion

3.1. Radiative Energy Balance

[17] Figure 2 illustrates the calculated clear and full sky heating rate profiles. The horizontal bars are a measure of geographical variability and measurement errors for each single profile. The assumed uncertainties are ±1 K in temperature, ±5% in ozone [*Thompson et al.*, 2003a] and ±30% in the mean water vapor profile. The altitude dependent error propagation from the measurement to the heating rate profile was estimated using mean tropical profiles disturbed according to the assumed uncertainty. For the two clear sky profiles, the transition from radiative cooling to heating occurs at 15 km, consistent with *Gettelman et al.* [2004]. In the UTLS, the profiles are shaped like an "S"

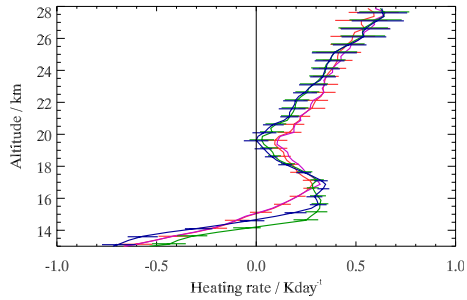

Figure 2. Calculated heating rate profiles. Red: clear sky based on 985 profiles of temperature and ozone combined with a mean water vapor profile. Magenta: clear sky based on a mean profile from all balloon sonde measurements at all seven locations. Green: full sky based on the 42 ISCCP types (subdivided in 250 m bins and 5 optical density bins, 1700 calculations in total) in combination with the mean balloon measurement profile. Blue: full sky based on 11,020 profiles from the combined LITE-ISCCP data set.

with a local maximum around the cold point tropopause (17 km) and a local minimum at 19.5 km. The small difference between the clear sky profile based on averaging 985 individual heating rate profiles (red curve) and the one based on a single radiative calculation for the mean temperature and trace gas profiles (magenta) reveals that nonlinear effects play a minor role in determining the mean radiative transfer. We utilize this property in our full sky calculation by assuming mean clear sky conditions for temperature and trace gases. The two profiles for full sky based on the ISCCP data (green curve) or the combined LITE-ISCCP data (blue curve) show qualitatively the same features as for clear sky.

[18] Above the cold point tropopause at 17 km altitude, the differences between the full and clear sky heating rate profiles are small; upwelling infrared radiation is partly absorbed by clouds and therefore not reaching the stratosphere, but this cooling effect is damped by the absorption of shortwave radiation reflected from the clouds. The main differences between the clear and full sky case are found in the troposphere. For the full sky case, the transition from radiative cooling to heating occurs 0.5–1.0 km lower than in clear sky. This result is at first sight surprising as air above dense clouds is cooled, which lets the level of zero net radiative heating rise [*Ramaswamy and Ramanathan*, 1989]. On the other hand, the air inside of thin high clouds without underlying optically thick clouds is heated due to infrared absorption. In the zonal average this in situ heating apparently dominates the cooling from underlying clouds, which is taken into account in our analysis. This leads to a lower level of zero net radiative heating and an enhanced heating between 15 and 17 km altitude.

3.2. Mass Flux Profiles

[19] Mean vertical mass fluxes for the heating rate profiles discussed in the previous section are presented in Figure 3. The error bars are based on the uncertainties described above plus 0.05 K day^{-1} for $\bar{\epsilon}$ in equation (2). Below 15 km the derived mass flux profile decreases rapidly, probably caused by the neglect of latent heat and turbulent mixing.

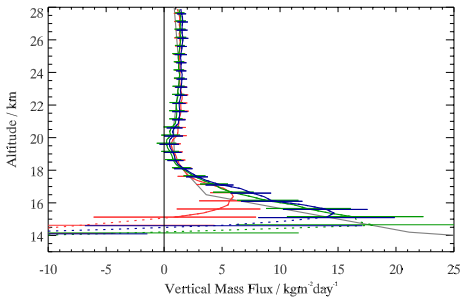

Figure 3. Mean vertical mass fluxes derived from the radiative transfer calculation for clear sky (red) and including the influence of clouds based on the ISCCP (green) and on the combined LITE-ISCCP data (blue). The grey curve represents the mean vertical mass flux from ECMWF ERA-15 reanalysis data.

[20] Above 17 km the clear (red curve) and full sky (green and blue curves) calculations yield decreasing mean mass flux with increasing altitude up to 18–19 km and almost constant mass flux above. Figure 3 shows that at most 20% of the air passing through the cold point tropopause at 17 km can reach the middle stratosphere. This finding is consistent with *Rosenlof et al.* [1997]. Below the cold point tropopause the mass flux derived from clear sky calculations is decreasing again, suggesting a mass convergence in the tropopause region. However, this feature has to be regarded as an artefact caused by the neglect of cloud radiative influences.

[21] The full sky mass flux profiles (green and blue curve) show no convergence in the UT, but a continuous divergence from 15 km up to 18–19 km. The mean mass flux derived from the calculation including the influence of clouds has to be regarded as the better estimate of the real mass flux in the atmosphere. Around 20 km, the full sky mass flux profile shows a minimum near zero. If this minimum was real, it would signify an almost complete decoupling of the circulation below and above this level. However, this feature is not significant, considering the uncertainties involved. The mass flux profile in the LS is well within the range of previous studies, whereas the results in the UT are the first available estimate derived from high-resolution measurements. The good agreement with the profile from ECMWF data (gray curve) shows the important contribution of cloud radiative heating to the vertical transport in the UTLS.

4. Conclusions and Outlook

[22] State-of-the-art radiation transport modeling in the tropical UTLS yielded divergent upwelling mean mass fluxes below 18–19 km. A considerable difference between the clear and full sky energy balance was found, demonstrating the importance of clouds in the UT. It can be concluded that the Brewer Dobson circulation - driven by an extra tropical wave drag - is the dominant process above an altitude of roughly 19 km. Below, other processes such as infrared cloud heating, extremely deep convection and wave dissipation must also be responsible for the upwelling.

[23] The present study quantified the mean vertical mass flux over several years and the whole equatorial region. Seasonal and geographical variabilities were not considered, but should be subject of future investigation. Moreover, there is a considerable uncertainty concerning the influence of clouds on the radiative energy budget due to limited information on cloud vertical structure and optical depth.

[24] More detailed cloud information will be available with the results from the lidar instrument (GLAS) on ICESAT and from the combination of lidar and radar systems on the future "A-Train". The transformed TEM framework could then be used to explore the seasonal and latitudinal variations of the vertical mass fluxes.

[25] **Acknowledgments.** ISCCP and LITE data were obtained from the NASA Langley Research Center Atmospheric Sciences Data Center. SHADOZ data were provided through the database available at http://croc.gsfc.nasa.gov/shadoz/. ECMWF ERA-15 data have been provided by MeteoSwiss. UKMO temperature data were provided through the SPARC Data Center at http://www.sparc.sunysb.edu/. TC thanks KA Powell for helpful comments on the LITE data. This work was supported by the Swiss Federal Office for Education and Science as part of TROCCINOX. QF is supported by NASA Grant NNG04GM23G and DOE Grant (Task Order 355043-AQ5 under Master Agreement 325630-AN4).

References

Boering, K. A., et al. (1996), Stratospheric mean ages and transport rates from observations of carbon dioxide and nitrous oxide, *Science*, *274*(5291), 1340–1343.

Comstock, J. M., T. P. Ackerman, and G. G. Mace (2002), Ground-based lidar and radar remote sensing of tropical cirrus clouds at Nauru Island: Cloud statistics and radiative impacts, *J. Geophys. Res.*, *107*(D23), 4714, doi:10.1029/2002JD002203.

Danielsen, E. F. (1993), In situ evidence of rapid, vertical, irreversible transport of lower tropospheric air into the lower tropical stratosphere by convective cloud turrets, *J. Geophys. Res.*, *98*(D5), 8665–8681.

Eluszkiewicz, J., et al. (1996), Residual circulation in the stratosphere and lower mesosphere as diagnosed from Microwave Limb Sounder data, *J. Atmos. Sci.*, *53*(2), 217–240.

Fu, Q., and K. N. Liou (1992), On the correlated k-distribution method for radiative-transfer in nonhomogeneous atmospheres, *J. Atmos. Sci.*, *49*(22), 2139–2156.

Gettelman, A., P. M. de F. Forster, M. Fujiwara, Q. Fu, H. Vömel, L. K. Gohar, C. Johanson, and M. Ammerman (2004), Radiation balance of the tropical tropopause layer, *J. Geophys. Res.*, *109*, D07103, doi:10.1029/2003JD004190.

Hartmann, D. L., L. A. Moy, and Q. Fu (2001), Tropical convection and the energy balance at the top of the atmosphere, *J. Clim.*, *14*(24), 4495–4511.

Holton, J. R., P. H. Haynes, M. E. McIntyre, A. R. Douglass, R. B. Rood, and L. Pfister (1995), Stratosphere-troposphere exchange, *Rev. Geophys.*, *33*(4), 403–439.

Liou, K. N. (1992), *Radiation and Cloud Processes in the Atmosphere*, 487 pp., Oxford Univ. Press, New York.

Mote, P. W., III (1998), Vertical velocity, diffusion, and dilution by midlatitude air in the tropical lower stratosphere, *J. Geophys. Res.*, *103*(D8), 8651–8666.

Newell, R. E., and S. Gould-Stewart (1981), A stratospheric fountain, *J. Atmos. Sci.*, *38*(12), 2789–2796.

Ramaswamy, V., and V. Ramanathan (1989), Solar absorption by cirrus clouds and the maintenance of the tropical UT thermal structure, *J. Atmos. Sci.*, *46*(14), 2293–2310.

Randel, W. J., et al. (1998), Seasonal cycles and QBO variations in stratospheric CH_4 and H_2O observed in UARS HALOE data, *J. Atmos. Sci.*, *55*(2), 163–185.

Rosenlof, K. H., and J. R. Holton (1993), Estimates of the stratospheric residual circulation using the downward control principle, *J. Geophys. Res.*, *98*(D6), 10,465–10,479.

Rosenlof, K. H., A. F. Tuck, K. K. Kelly, J. M. Russell III, and M. P. McCormick (1997), Hemispheric asymmetries in water vapor and inferences about transport in the lower stratosphere, *J. Geophys. Res.*, *102*(D11), 13,213–13,234.

Rossow, W. B., and R. A. Schiffer (1999), Advances in understanding clouds from ISCCP, *Bull. Am. Meteorol. Soc.*, *80*(11), 2261–2287.

Sohn, B. J. (1999), Cloud-induced infrared radiative heating and its implications for large-scale tropical circulations, *J. Atmos. Sci.*, *56*(15), 2657–2672.

Thompson, A. M., et al. (2003a), Southern Hemisphere Additional Ozonesondes (SHADOZ) 1998–2000 tropical ozone climatology: 1. Compar-

ison with Total Ozone Mapping Spectrometer (TOMS) and ground-based measurements, *J. Geophys. Res.*, *108*(D2), 8238, doi:10.1029/2001JD000967.

Thompson, A. M., et al. (2003b), Southern Hemisphere Additional Ozonesondes (SHADOZ) 1998–2000 tropical ozone climatology: 2. Tropospheric variability and the zonal wave-one, *J. Geophys. Res.*, *108*(D2), 8241, doi:10.1029/2002JD002241.

Trenberth, K. E. (Ed.) (1993), *Climate System Modeling*, 817 pp., Cambridge Univ. Press, New York.

Volger, P., Z. Y. Liu, and N. Sugimoto (2002), Multiple scattering simulations for the Japanese space lidar project ELISE, *IEEE Trans. Geosci. Remote Sens.*, *40*(3), 550–559.

Vömel, H., et al. (2002), Balloon-borne observations of water vapor and ozone in the tropical upper troposphere and lower stratosphere, *J. Geophys. Res.*, *107*(D14), 4210, doi:10.1029/2001JD000707.

Wang, P. H., et al. (1998), A study of the vertical structure of tropical (20S–20N) optically thin clouds from SAGE II observations, *Atmos. Res.*, *48*, 599–614.

Winker, D. M., R. H. Couch, and M. P. McCormick (1996), An overview of LITE: NASA's lidar in-space technology experiment, *Proc. IEEE*, *84*(2), 164–180.

T. Corti, B. P. Luo, and T. Peter, Institute for Atmospheric and Climate Science, ETH, Honggerberg HPP, CH-8093 Zurich, Switzerland. (tcorti@env.ethz.ch)

Q. Fu, Department of Atmospheric Sciences, University of Washington, 408 ATG Bldg., Seattle, WA 98915-1640, USA.

H. Vömel, Cooperative Institute for Research in Environmental Sciences, University of Colorado, 325 Broadway, Boulder, CO 80303, USA.